Red blood cell and platelet diffusivity and margination in the presence of cross-stream gradients in blood flows

Závodszky, G.; van Rooij, B.; Czaja, B.; Azizi, V.; de Kanter, D.; Hoekstra, A.G.

DOI
10.1063/1.5085881

Publication date
2019

Document Version
Final published version

Published in
Physics of Fluids

Physics of Fluids ARTICLE scitation.org/journal/phf

Red blood cell and platelet diffusivity and margination in the presence of cross-stream gradients in blood flows

Cite as: Phys. Fluids 31, 031903 (2019); doi: 10.1063/1.5085881
Submitted: 16 December 2018 • Accepted: 19 February 2019 •
Published Online: 12 March 2019

Gábor Závodszky,[1,2,a)] Britt van Rooij,[1] Ben Czaja,[1] Victor Azizi,[1] David de Kanter,[1] and Alfons G. Hoekstra[1,3]

AFFILIATIONS

[1]Computational Science Lab, Faculty of Science, Institute for Informatics, University of Amsterdam, Amsterdam, The Netherlands
[2]Department of Hydrodynamic Systems, Budapest University of Technology and Economics, Budapest, Hungary
[3]ITMO University, Saint Petersburg, Russia

[a)]**Electronic mail:** g.zavodszky@uva.nl

ABSTRACT

The radial distribution of cells in blood flow inside vessels is highly non-homogeneous. This leads to numerous important properties of blood, yet the mechanisms shaping these distributions are not fully understood. The motion of cells is governed by a variety of hydrodynamic interactions and cell-deformation mechanics. Properties, such as the effective cell diffusivity, are therefore difficult to investigate in flows other than pure shear flows. In this work, several single-cell, cell-pair, and large-scale many-cell simulations are performed using a validated numerical model. Apart from the single-cell mechanical validations, the arising flow profile, cell free layer widths, and cell drift velocities are compared to previous experimental findings. The motion of the cells at various radial positions and under different flow conditions is extracted, and evaluated through a statistical approach. An extended diffusive flux-type model is introduced which describes the cell diffusivities under a wide range of flow conditions and incorporates the effects of cell deformability through a shear dependent description of the cell collision cross sections. This model is applicable for both red blood cells and platelets. Further evaluation of particle trajectories shows that the margination of platelets cannot be the net result of gradients in diffusivity. However, the margination mechanism is strongly linked to the gradient of the hematocrit level. Finally, it shows that platelets marginate only until the edge of the red blood cell distribution and they do not fill the cell free layer.

I. INTRODUCTION

Blood is a dense mixture of deformable cells and proteins suspended in blood plasma. Its complex, non-Newtonian rheology arises from these components. Red blood cells (RBCs) have the highest concentration of about 40%–42% in a healthy human, outnumbering platelets (PLTs) by 10:1 and white blood cells (WBCs) by 500:1.[1,2] Flowing in vessels, each cell species displays a non-homogeneous distribution along the radius of the vessel. The mechanisms that lead to lateral cell migration have been heavily investigated. This includes studies on immersed droplet mechanics, focusing on the hydrodynamic interactions,[3–7] and studies aiming specifically at blood cells to show the influence of various cell properties, such as shape, size, rigidity, and viscosity contrast.[8–11] Apart from the cells, the domain geometry also plays an important role. Confinement was shown to cause deformable cells to migrate away from the boundary.[6,12,13] For instance, RBCs migrate away from the vessel wall which creates a red blood cell free layer (CFL) of plasma that acts as a lubrication layer around the cellular flow. As an implication, a decreasing diameter of vessels gives rise to lower bulk viscosities (Fåhræus–Lindqvist effect[14]). This tendency stops when the vessel diameter approaches the RBC diameters, at which point the bulk viscosity starts to increase again steeply.[15] A further implication is that the actual hematocrit flowing in small vessels

(tube hematocrit) is lower than the discharge (or tank) hematocrit,[15] which is called the Fåhræus effect. Moreover, a size exclusion effect applies for blood cells flowing very close to the vessel wall. On one hand, they have a finite size; therefore, their center of mass cannot get closer to the boundary than their actual radius. On the other hand, *in vivo* vessels are lined with a layer of macromolecules (i.e., glycocalyx) that protrudes in the plasma flow and prohibits the flowing of larger cells, such as RBCs.[16] The curved velocity profile of the blood flow inside vessels also induces a lift force on cells. For rigid spherical objects, this drives particles towards the $0.6 * R$ radial position (Segré-Silberberg effect), while for deformable cells, this force points towards the center of the channel.[17,18] This is the dominant effect that causes an increased hematocrit and even overcrowding of RBCs around the middle of the channel in smaller vessels.[19–21] At vessel bifurcations, a combination of these effects leads to plasma skimming and cell screening,[16,22] and the non-trivial distribution of local viscosity.[23]

An important remaining question is the description of cell-cell interactions. While several numerical studies investigated the intensity of cell diffusivity and cell margination[24–26] under various flow conditions, they generally report trends without examining the mechanical root causes in detail. When blood is subject to a non-zero shear flow, the interaction between cells leads to an increased diffusive behaviour surpassing the thermal diffusion of the cells by several orders of magnitude.[27–29] This shear-induced diffusion manifests in two ways. First, the consecutive collisions of a cell with other cells cause repeated displacements, which results in a random walk-like behaviour with a zero net flux (self-diffusion). And second, the inhomogeneities in concentration and flow conditions yield an additional term in diffusivity that has a non-zero net flux (gradient-diffusion).[13,30,31] In practice, these two effects are often investigated together as it is difficult to separate them. They have a significant contribution to the trafficking of immersed particles. In fact, the inhomogeneous distributions of platelets and white blood cells are attributed primarily to hydrodynamic interaction with the dominant species (RBCs). Their lateral motion is defined by a series of cell-cell collisions which are shown to depend on deformability, relative size, and number density.[10,32–34] The motion of smaller particles (e.g., platelets), therefore, is usually approximated using either drift-diffusion type equations[35,36] or stochastic approaches. For instance, the trajectory of a particle can be viewed as a stochastic series of collisions forming a Markov chain where the evolution of the probability density function is described by the Fokker-Planck equation.[36,37]

Several numerical investigations have targeted these questions to provide more detailed insight into the collision events. These techniques typically rely on immersed boundary simulations,[11,38–40] the boundary integral method,[41,42] or dissipative particle dynamics.[43,44] Despite these efforts, a robust framework that can fully describe the shear-induced diffusive behaviour of a dense mixture of deformable particles is currently not available. Several models have been proposed for simplified systems, such as monodisperse suspensions for hard spheres. One well-known model is the diffusive flux model introduced by Leighton and Acrivos,[27] which was later further refined by Phillips *et al.*[45] by introducing irreversible particle interactions. Recently, it was extended to bidisperse suspensions of rigid spheres.[46] Another phenomenological model is the suspension balance model that describes fluxes associated with particle collisions.[47,48] While these idealised models progress our understanding of the governing mechanisms, they are so far unable to provide quantitative predictions that are in full agreement with the experimental results.

In the current work, several cellular blood flow simulations are performed to evaluate the detailed diffusive behaviour of the cells. Since many of the aforementioned mechanisms cannot be reproduced in pure shear flow, the study is based on both pure shear and body-force driven straight channel flows of up to 1 s of flow with varied shear rates and hematocrit levels. Single-cell mechanics and emerging bulk properties are compared to previous experimental results to ensure the validity of the computations. And finally, an extended drift-diffusion model is proposed that takes cellular deformation due to local flow conditions into consideration.

II. METHODS

A. Numerical methods

The cellular flow is simulated with the HemoCell software.[40,49] It is based on a combination of the lattice Boltzmann method (LBM) which has been shown to reproduce accurate flow fields in vascular settings[50–53] and a high-performance implementation of the immersed boundary method (IBM).[54,55] The blood plasma is represented as an incompressible Newtonian fluid, and the cells are modelled as triangulated membrane meshes immersed in the plasma flow. Out of the more wide spread phenomenological models,[40,44,56,57] the one introduced by Závodszky *et al.*[40] is employed in the current work due to its improved mechanical behaviour in the case of sustained shear rates over 1500 s^{-1}. In the current work, we employ the same parameters as reported in Ref. 40, where the detailed description of this model and its numerical implementation can be found. Two different flow configurations are considered: pure shear flows to investigate single-cell deformations and cell-cell pair interactions, and body force driven straight channel flows. The latter allows the incorporation of the effects resulting from the complex bulk behaviour of blood in the presence of gradients. Computationally, these are large-scale simulations, each of which was run on 256 computing cores for up to 10 days of wall clock time to accurately resolve 1 s of flow.

For the validation of the single-cell mechanics, we refer the reader to the work of Závodszky *et al.*,[40] where the deformation of single RBCs due to stretching and shearing was thoroughly investigated and compared to experimental results and other numerical models. It was found that the shape of the sheared model RBC reproduced very well that of the healthy human RBC. Furthermore, the same work contains validation of collective cellular flow behaviour of the model in straight channels regarding the emergent bulk viscosity, cell free layer, and flow profile. Due to the significance of the latter in relation to the current work, the comparison of emerging flow profiles has been reproduced from previous simulation data here. In the work of Carboni *et al.*,[58] tracking particles were used to make the velocity profile visible in a straight rectangular channel flow of high hematocrit blood (H = 35%). In Fig. 1, a comparison is shown between the experiments and the velocity profile computed with HemoCell using the same geometry, hematocrit level, and boundary conditions. The results are in good agreement with the experiments, which indicates the good accuracy of the model.

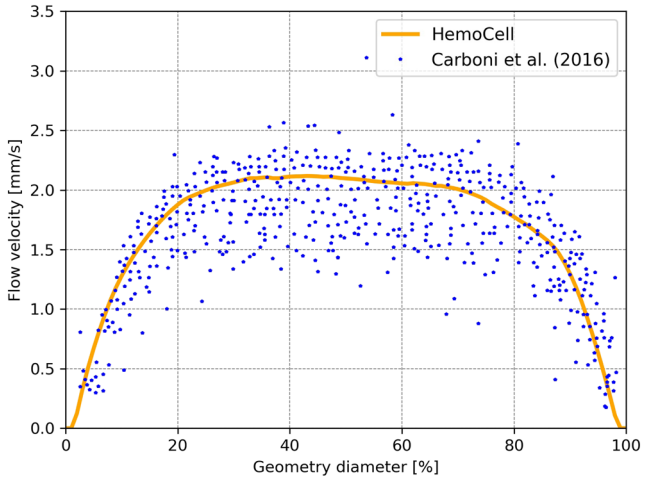

FIG. 1. Comparison of cross-channel flow velocity profiles between the current numerical method and experiments[58] at $H = 35\%$. The average distance of the measurement points from the simulated profile is $\overline{\Delta v} = 0.15$ mm/s.

B. Extended diffusivity model

The effective diffusivity of monodisperse particles in a confined suspension flow is influenced by three different length scales: first, the characteristic size of the colliding particles, which is generally taken as the radius, then, the typical distance between particles, and finally, the distance from the wall.[29] In dilute suspensions far from the boundaries, the dominant length scale is the characteristic particle size. In this case, several scaling studies suggest[4,21,30,59] that the shear-induced diffusivity takes the following form:

$$D = Ca^2 \dot{\gamma} \Phi, \tag{1}$$

where $\dot{\gamma}$ is the shear rate, Φ is the volume fraction, a is a characteristic length scale of the particle (e.g., the radius), and C denotes a parameter dependent on the shape and material properties of the particles. The latter is usually estimated from experimental observations.[13] However, since RBC dynamics and deformation depend on the shear rate,[12,13,60] apart from the low shear rate cases, the effects of cell deformation must be taken into account. To do this, Eq. (1) needs to be extended. The amount of cell displacement over time can be approximated along the ideas of the diffusive flux model as being proportional to the frequency of collisions. The frequency of collisions is, in turn, proportional to the size of the collision cross section, the relative velocity of the particles on a collision trajectory (i.e., the shear rate), and the volume fraction. Recently, Rosti *et al.*[61] showed the importance of shear-induced cross section change of elastic deformable capsules in terms of the emergent viscosity of the sheared system. Here, we argue that the shear-induced deformation of RBCs is also important in terms of the appearing diffusivity. Furthermore, the effects of this deformation can be approximated through the changes in the collision cross section. A moderate hematocrit level where the pair-collisions dominate is assumed, and the effect of collisions between three or more cells is neglected. The collision cross section for two cells is defined as

$$\sigma(\dot{\gamma}) = \pi\left[r_1(\dot{\gamma}) + r_2(\dot{\gamma})\right]^2, \tag{2}$$

where r_1 and r_2 denote the shear dependent collision radius of the two cells in the direction of the shear gradient. Note that the two cells can belong to different species.

Incorporating the collision cross section in Eq. (1) leads to the extended form of shear-induced diffusivity

$$D = C'\sigma(\dot{\gamma})\dot{\gamma}\Phi, \tag{3}$$

where C' is a shear rate independent fitted parameter, unique to the colliding cell type pairs. In our computations, the cell radii are defined as

$$r_{PLT} = 1.2\,\mu\text{m},$$

$$r_{RBC}(\dot{\gamma}) = 3.92\,\mu\text{m} \cdot D_{norm}(\dot{\gamma}),$$

where $D_{norm}(\dot{\gamma})$ is the normalised RBC diameter which is used to define the collision radius. This collision radius of a single RBC in shear flow as a function of shear rate is shown in Fig. 2. This curve was extracted from simulations using HemoCell up to $\dot{\gamma} = 4000\ \text{s}^{-1}$, which is higher than the highest appearing shear rate value in the subsequent simulations. It shows a steep deformation curve that agrees well with both experimental and previous computational observations[62,63] (for further details, see the Wheeler test validation in Ref. 40). For the rest of the current work, we use this curve to define the shear dependent diameter of RBCs for the collision cross sections. We also provide a fitted function that matches the simulated results closely in the form of $a \cdot e^{-b\dot{\gamma}} + c$, where $a = \frac{1}{1.6}$, $b = 0.0013$, $c = \frac{0.6}{1.6}$, with a mean square error $=5 \times 10^{-4}$ (shown in Fig. 2).

C. Cell collision simulations

We focus on cell displacement from an isolated cell pair-collision event where at least one of the cells is deformable. The displacement after the collision is strongly dependent on the capillary number.[10,34,42] Such a collision setup is depicted in

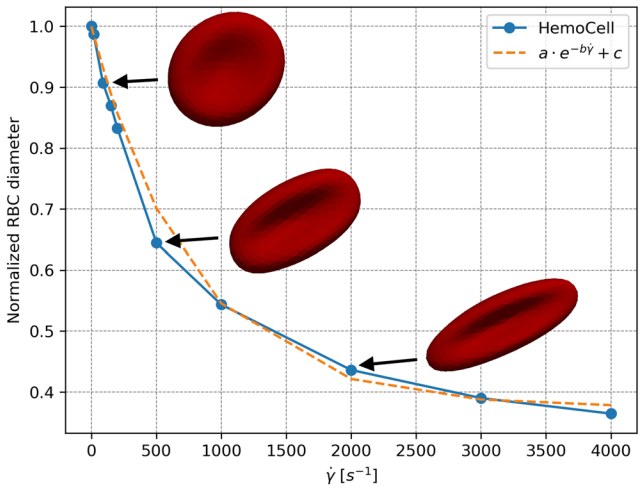

FIG. 2. Normalised collision diameter of an RBC in pure shear as a function of shear rate. The dashed line denotes the fitted function of $a \cdot e^{-b\dot{\gamma}} + c$, where $a = \frac{1}{1.6}$, $b = 0.0013$, $c = \frac{0.6}{1.6}$.

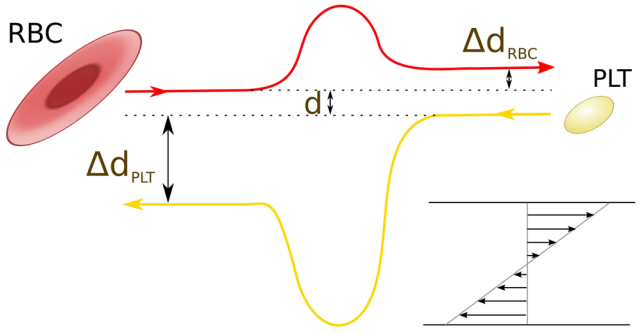

FIG. 3. Schematic overview of an RBC-platelet pair collision in shear flow. The distance between the centre of mass of the colliding cells is denoted as d, and Δd denotes the displacement of the centre of mass of a cell after the collision.

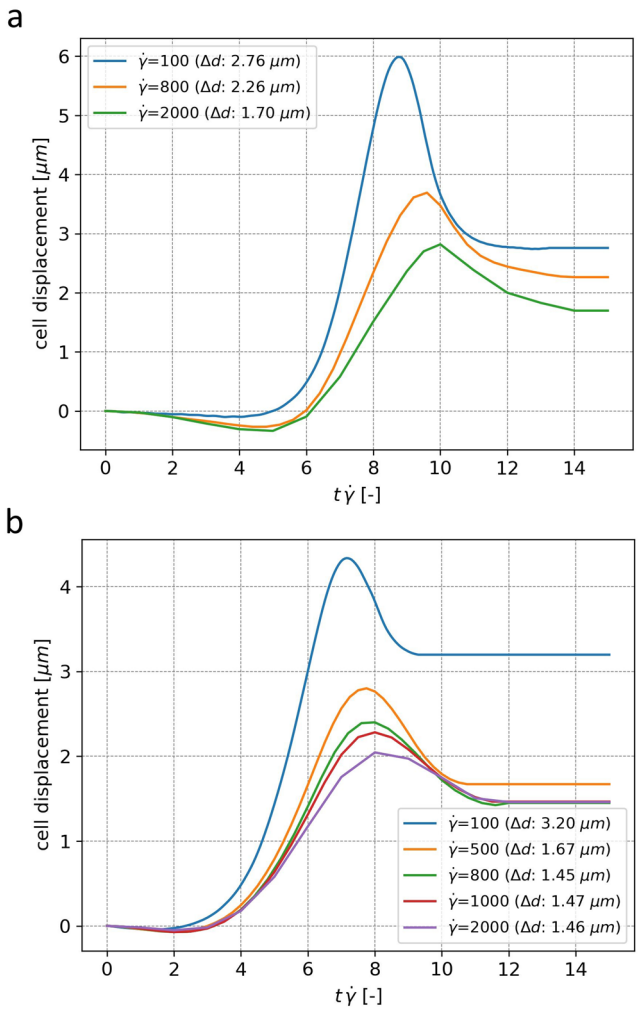

FIG. 4. Resulting cell displacement during a cell pair collision in pure shear, with the original cell core distance (d) of 2 μm. The total displacement between before and after the collision is denoted Δd. (a) Platelet displacement of an RBC-platelet collision. (b) RBC displacement of an RBC-RBC collision.

Fig. 3. The cell types of interest in the current work are RBCs and platelets with RBCs being the significantly more numerous species. Due to this, collisions not involving at least one RBC are neglected. We show RBC-RBC and RBC-platelet collision events in Fig. 4.

As a limiting case, rigid sphere binary collisions in Stokes flows are time reversible. In our case, the time symmetry does not hold due to the deformability of the RBCs (the effect of surface roughness and of protein chains in plasma[64,65] is not modeled). In an RBC-PLT pair collision, as expected based on cell mass differences, the RBC is barely affected (<0.1 μm typical displacement). Meanwhile, the platelet is forced to a trajectory around the RBC during the collision resulting in a larger displacement, which is proportional to the common collision radius of the two cells. For lower shear rate cases, the amount of deformation is limited; therefore, the collision in principle is closer to the rigid sphere case than the ones with high shear rate. During the collision, as shown in Fig. 4(a), the platelet displaced up to 6 μm, but right after the collision it settles back to around 2.7 μm. This returning trajectory is not so pronounced in higher shear cases and in RBC-RBC collisions [Fig. 4(b)] where there is more deformation involved. In general, with the increase of shear

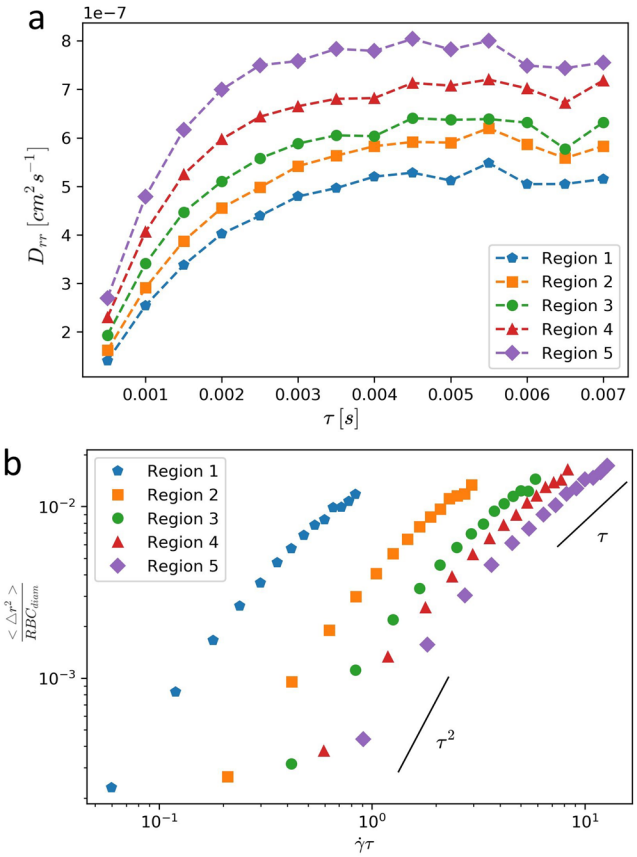

FIG. 5. Mean square displacement curves of RBC trajectories in five different coaxial volumes within a straight tube flow. Region 1 is in the middle of the tube, while Region 5 is next to the wall. (a) Values of Eq. (4) as a function of τ. (b) Normalised mean square displacement as a function of strain.

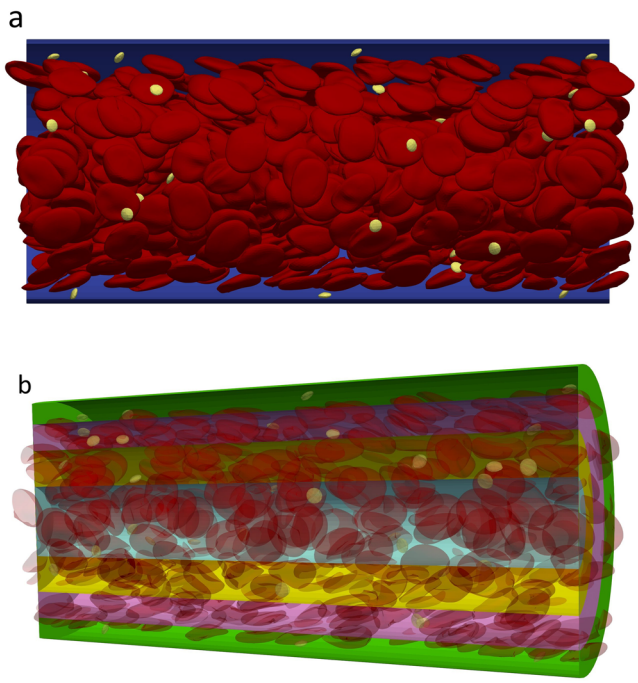

FIG. 6. (a) Visualisation of a periodic straight cylindrical channel flow computation of about 620 cells after 1 s of flow with marginated platelets. (b) Visualisation of four coaxial layers in the same simulation.

rate the final displacement of the cells decreases. This trend is partly driven by the decreasing radius of the RBCs in the shear gradient direction (i.e., collision radius) due to deformation in the sheared environment.

D. Cylindrical channel flow simulations

We calculate the effective diffusivity of particles from their trajectories. For a large enough time-window (τ), the diffusivity (i.e., tracer diffusivity) of particles in the x direction can be estimated from their displacement during τ time[66–68]

$$D_{xx} = \frac{1}{N}\sum_{i=1}^{N}\frac{\langle (x_i(\tau) - x_i(0))^2 \rangle}{2\tau}, \tag{4}$$

where N denotes the number of tracked particles. The τ time-window has to be large enough to incorporate several collision events, otherwise Eq. (4) represents ballistic behaviour of the cells and will be quadratic in time. The choice of the appropriate time-window depends on the shear rate, and it scales as $\tau \sim 1/\dot{\gamma}$.

TABLE I. List of the parameter values for Re(—) and H(%) in cylindrical channel flows of $D = 50\ \mu$m diameter. In total 15 channels, flow simulations have been carried out using these value pairs.

Re	0.04	0.4	0.4	0.5	0.5	1.0	1.0	1.0	1.5	1.5	1.5	1.7	2.0	2.0	2.0
H	10	7	10	27	35	10	27	35	10	27	35	35	10	27	35

To make sure that we evaluate trajectories in the diffusive regime we fine-tuned τ for every computation. An example of such a tuning is shown in Fig. 5 for five different coaxial regions, with each forming a hollow cylindrical volume. These volumes fill the full cylindrical channel like onion layers, and they represent regions of different shear rate and hematocrit values in the flow [for a visualisation of such coaxial volumes, see Fig. 6(b)].

The pressure driven flow of the straight capillary tube includes up to 620 cells [see Fig. 6(a) for an overview]. The diameter of the channel is $D = 50\ \mu$m, and the two varied parameters are the Reynolds number and the hematocrit. The combination of these parameters is listed in Table I. They cover the widest physiological range that might arise in either venous or arterial microcirculation.

We focus on the radial diffusivity D_{rr} (i.e., the diffusivity in the shear gradient direction), as the diffusivity in the vorticity direction is typically at least an order of magnitude smaller than the radial diffusivity.[69–71] Furthermore, we neglect thermal diffusivity based on the Stokes-Einstein equation. For micron-sized particles in blood plasma, it predicts a Brownian motion at least two orders of magnitude smaller than the shear-induced diffusivities.

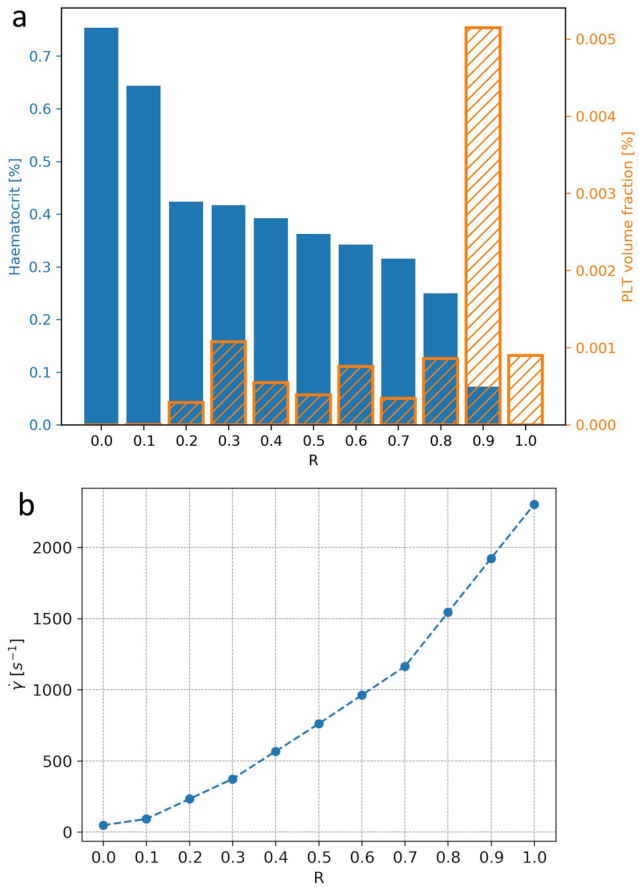

FIG. 7. (a) RBC and PLT volume fraction profiles. (b) Shear rate profile in the same simulation (tube flow of $D = 50\ \mu$m, $H_D = 35\%$, $Re = 1.5$). R denotes the normalised radial position.

Radial diffusivity is calculated from the trajectories of the cells using Eq. (4). The whole domain of the tube is subdivided into eleven coaxial regions along the radius [similarly to Fig. 6(b)], and all the reported values are averaged in time (100 ms window) and in space within these regions. The shear rate is calculated in every fluid node within the region before averaging, and the hematocrit is calculated using the number of RBC center of masses within a region. The width of these regions corresponds to the size of the platelets (≈2.5 μm). This choice on one hand necessitates a large sample number to reduce the noise, but on the other hand, it enables us to investigate the effects of cell-scale gradients. This way PLTs will often and RBCs will always overlap with multiple regions of different hematocrit and shear values.

An example of an emerging hematocrit and platelet volume fraction profile with flow shear rate along the radius is shown in Fig. 7 based on these regions. Note that the peak in the hematocrit in the middle of the tube is more pronounced for vessels of small radius, due to the larger relative wall effects and wall induced lift. In larger simulated channels with D = 80 μm and 128 μm at similar overall hematocrit values, the peak disappears and the center region of the profile smoothens out. In smaller diameter flows, however, there is always a small volume of the low shear rate and high hematocrit in the middle in accordance to previous findings.[19,37] The case in Fig. 7 is from a simulation of Re = 1.5 and H = 35% where the trajectories are evaluated from t = 0.5 s to t = 1.0 s.

III. RESULTS

A. Radial diffusivity

Two additional comparisons have been made with experimental results to assess the accuracy of the diffusivity computations. In the rectangular channel flow discussed in Ref. 58 (see also Sec. II A), the diffusion coefficient of spherical tracer particles (D = 2.11 μm) averaged over the channel was found to be approximately 0.15 × 10^{-6} cm^2 s^{-1}. Under the same flow conditions, platelets in our computations yield a close value of 0.24 × 10^{-6} cm^2 s^{-1}. In a much slower channel flow of 10% hematocrit,[72] the tracer particle diffusivity was found to be 8.5 × 10^{-9} cm^2 s^{-1}. Our computational replica of that experiment yields a value of 7.54 × 10^{-9} cm^2 s^{-1} for platelets. Note that there might be differences arising from the shape since the tracer particles in the experiments are spherical, while our platelets are ellipsoidal.

Using the results of the other 15 simulations, the parameter C' of Eq. (3) can be inferred by correlating the model predictions with the effective diffusivities that are extracted from the cell trajectories using Eq. (4). In the following, we define C' with the help of a fitting coefficient a as $C' = \frac{a}{\sigma(\dot{\gamma}=0)}$. Figure 8 shows the fitting to the simulation results. In this figure, every data point represents an average value within a different region (i.e., a coaxial volume) in one of the simulations. The model uses the local hematocrit and shear rate values from that specific region, while D_{rr} describes the effective diffusivity of the same region based on cell trajectories. The regions in the center of the channel flows (around R = 0) are excluded from the fit, as the hematocrit in these volumes is extremely high. Here a different scaling is expected[13,73] due to cell clustering and volume exclusion effects. The two volumes next to the vessel wall, denoted by black triangles, are also excluded since they cover mostly the cell free layer where RBCs are absent. Therefore, we have too few trajectories for RBCs and the diffusivity for platelets comes from their tumbling in high shear. Those few RBCs appearing in the CFL region present low average diffusivities that are mostly associated with lift force generated movement. The fit for RBCs yields a_{RBC} = 0.81 cm^2 with a linear correlation coefficient of 0.92, and for platelets a_{PLT} = 1.02 cm^2 with an even higher linear correlation coefficient of 0.96.

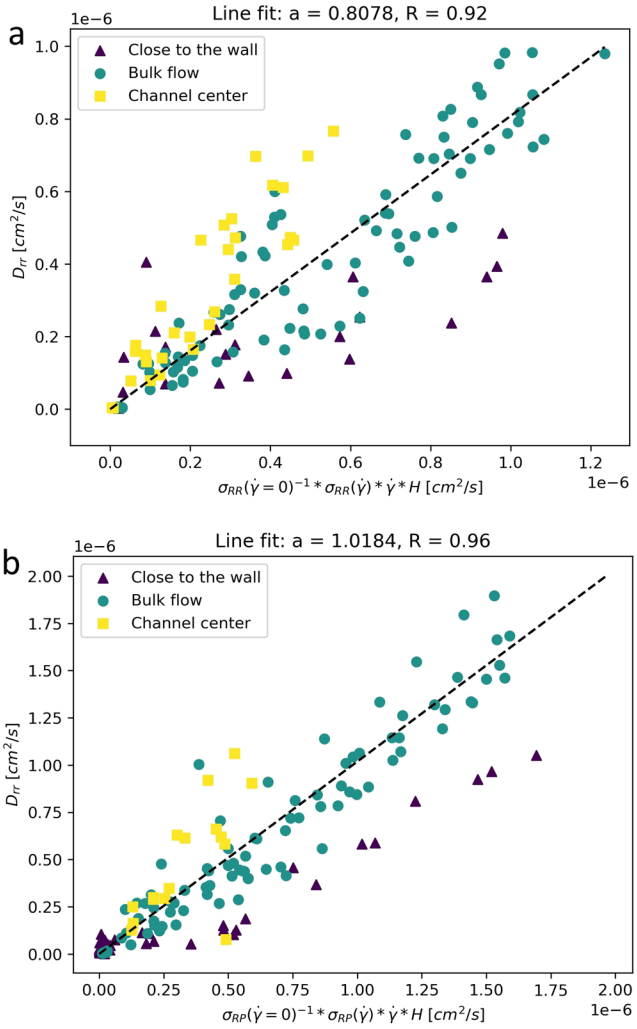

FIG. 8. Correlation between the modelled radial diffusivity [based on Eq. (3)] for RBCs (a) and PLTs (a). The yellow squares correspond to regions in the middle of the channel with high hematocrit and the black triangles show regions close to the wall. These two regions are not expected to follow the model predictions.

Next, we can use these fitted values to compare the model predictions of Eq. (3) to trajectory-extracted diffusivities along different radial positions. Figure 9 shows a representative example for the Re = 1.5, H = 35% channel flow, where Fig. 9(a) corresponds to RBC diffusivities and Fig. 9(b) shows the same for PLTs.

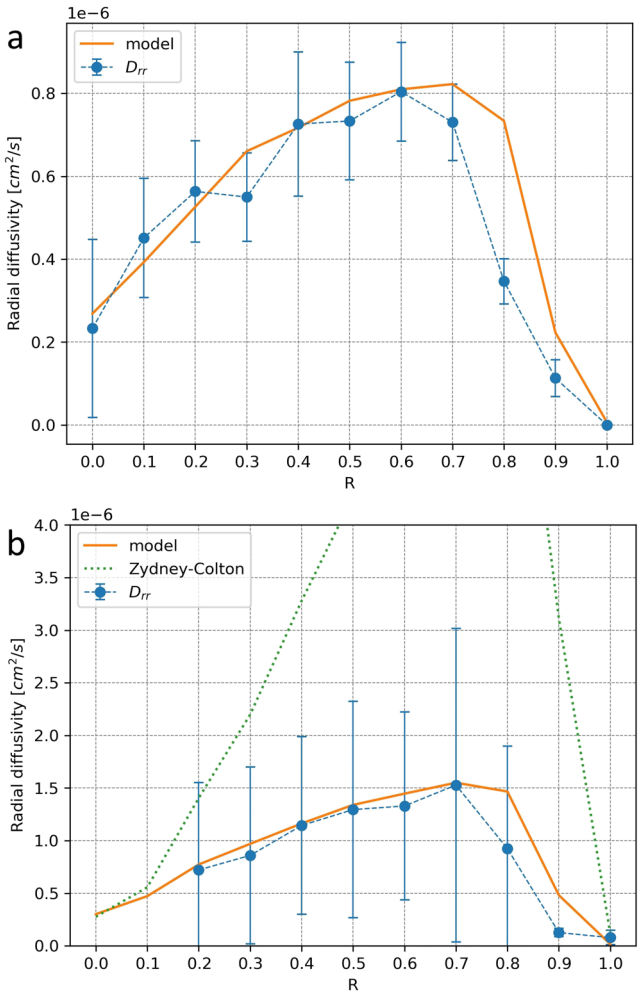

FIG. 9. Comparison between the radial diffusion inferred from the particle trajectories according to Eq. (4) and the model predictions of Eq. (3) along the radius of the vessel with Re = 1.5, H = 35%. (a) RBC radial diffusivities and (b) PLT diffusivities. The error bars represent the standard deviations. R denotes the normalised radial position.

The PLT diffusivity is also compared to the approximations of the Zydney-Colton model, which was found to overestimate platelet diffusivity significantly in regions of high shear rates. Note that cell diffusivity values for platelets have larger standard deviations than the values for RBCs. The reason is that platelets marginate outwards from the flow, and once they leave a region they rarely return. Therefore, the amount of samples they generate in a region is limited.

The discrepancy around R = 0.8 arises from the numerical method of averaging within the regions, and it scales with the size of the regions (i.e., the numerical resolution). The reason is that the discretization cannot capture the exact location of the steep gradient of the hematocrit at the edge of the CFL. Otherwise, the model shows good agreement for both cell types. Note that for the platelets, the D_{rr} values are absent in the centre of the channel since in the case of high hematocrit they are pushed out from that region quickly.

B. Drift velocity

The average drift velocity of the particles can also be extracted form the trajectory samples similarly to Eq. (4),

$$V_{xx} = \frac{1}{N}\sum_{i=1}^{N}\frac{\langle x_i(\tau) - x_i(0)\rangle}{\tau}. \tag{5}$$

For RBCs, the average drift velocity fluctuates around zero when the hematocrit profile equilibrates in 50–100 ms after start-up from a random homogeneous initial distribution. Afterwards, the net flux of gradient diffusivity balances the flux caused by the drift arising from cell overcrowding in the middle of the channel and from lift forces due to wall effects and flow profile curvature. This balance mechanism was also demonstrated recently in the work of Qi and Shaqfeh.[74] For platelets, however, there is no stable balance inside the bulk flow, and the acting forces result in a positive overall flux towards the wall. Figure 10 shows the average drift velocity profile from the Re = 1.5, H = 35% simulations along the radial regions. The qualitative shape is similar for all cases which allows for general observations. A high peak of the drift velocity is observed in the centre of the channel (R = 0). The corresponding sample trajectories originate mostly from the early phases of the simulations since platelets vacate this region quickly with the increase of the local hematocrit. There are previous findings, where platelet trajectories also showed short initial inward migration.[37] This effect is absent in our computations most likely due to the well mixed initial conditions of the system using the method developed in our previous work.[40] The negative drift at the wall (R = 1.0) is again an early phase phenomenon, caused by platelets that were put flat next to the wall during the initial condition generation. The lift force generated on these by rolling on the wall surface quickly drives them inwards where they start to tumble. Experimental findings[58] show an average tracer particle drift of V_{drift} = 0.0017 cm/s for flow conditions within our parameter range. While direct comparison is not feasible, if we disregard the two regions with early stage artefacts (R = 0 and 1.0), the computation of Re = 1.5, H = 35% falls close in flow conditions and presents an average platelet drift of $<V_{drift}>$ = 0.0019 cm/s (see the radial profile in Fig. 10). Looking at the general properties of the function, the drift velocity tends to zero as we approach the edge of the CFL where the platelets start to accumulate. There is one more region around R = 0.6 where the drift is typically low. Indeed, comparing it to the platelet profile in Fig. 7(a), we see a slighter PLT accumulation here as well. By the end of the computations, most of the PLTs reside in or at the edge of the CFL. The radial trajectories of a few randomly selected platelets from the simulation Re = 1.5, H = 35% are shown in Fig. 11, where the accumulation around R = 0.6 is also apparent. The edge of the CFL for this case is denoted by a dashed line, and the width of it agrees with the experimental measurements.[75] Platelets are marginated towards this region and eventually, after 0.9 s, they reside either in the CFL or around R = 0.6, the two places with close to zero drift in Fig. 10. Furthermore, platelets do not fill the CFL homogeneously, rather they aggregate on the edge of the RBC filled domain, periodically penetrating into the low hematocrit layers.

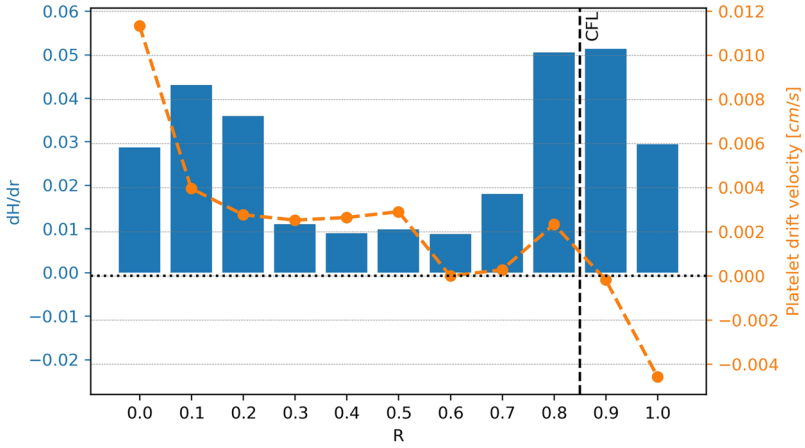

FIG. 10. Drift velocity (V_{rr}) profile of PLTs (dashed line) and hematocrit gradient (bars) from the simulation Re = 1.5, H = 35% [the hematocrit profile is shown in Fig. 7(a)]. R denotes the normalised radial position. While local drift values vary based on the hematocrit and shear rate, the overall qualitative shape of the curve is similar for every channel flow simulation.

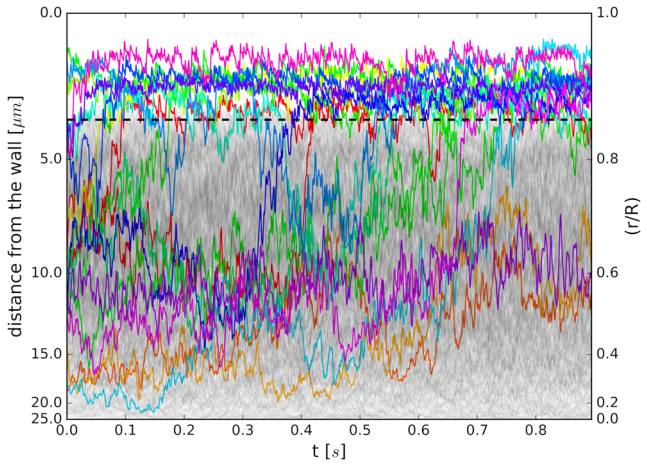

FIG. 11. Radial trajectories (coloured lines) of randomly selected platelets with RBC trajectories (grey lines) as background. The dashed line indicates the edge of the cell free layer. Note that the radial scale is quadratic to maintain the correct volume density of cells in the plot.

IV. DISCUSSION AND CONCLUSIONS

Cell pair collision simulations (for instance, in Fig. 3) show that the outcome of the collision is dependent on the local shear rate. The amount of cell displacement is directly influenced by the changed cross section of the cells. This in turn has effect on the diffusive behaviour. This leads to two competing processes. An increase in shear rate increases the collision frequency of the cells, while at the same time it decreases their collision radius. The proposed model based on Eq. (3) captures this by allowing the collision radius of the cells to vary as a function of shear rate. When comparing our results to the model of Zydney-Colton, we find a very good agreement between the models for low shear (i.e., below 100 s^{-1}) where RBC deformations are small. However, for higher shear rate zones, the Z-C model can overestimate diffusivity significantly (up to a factor of 5–10 in our cases).

There are two limitations, however, to our proposed model. In high hematocrit regions (above 40%–45%), our model assumptions are no longer accurate, as they lead to an underestimation of the diffusivities (see, e.g., the yellow squares in Fig. 8). In the work of Mountrakis *et al.*,[73] a scaling of $\sim \dot{\gamma}^{1/2}$ was found in a constant shear 2D system, which we cannot confirm for the current channel flows as it would lead to even stronger underestimation of D_{rr} values. Grandchamp *et al.*[13] suggested a scaling of $\sim H^2$ for high hematocrit Poiseuille flows by including three particle collisions, which might explain the increased diffusion. Apart from this, the diffusivity on the edge of the CFL is not fully captured. The cell dynamics here is different since collision events from one side of the cells are much more frequent. The two balancing processes for RBCs are therefore the deformation induced lift against the displacement from the one-sided collisions.

Platelets in our simulations marginated to the edge of the RBC rich domain, in accordance to the findings of Vahidkhah *et al.*[76] As observed in Fig. 7(a), the platelets mostly reside at R = 0.9, mixed with the dilute RBC layer, periodically penetrating the close higher hematocrit region and then drifting back to the edge of the CFL. Previous studies hypothesised that platelet margination is primarily the result of the gradients in platelet diffusivity.[35,45] In our simulations, platelet drift manifests as a small skewness on the distribution of PLT displacements, which results in a non-zero mean. That is, the result of multiple cell collisions and hydrodynamic interactions in the presence of gradients is not purely diffusive. Note that even if the relative magnitude of this skewness is small, it might still influence the calculation of D_{rr}. When we included corrections (i.e., subtracted the mean drift from individual displacements), it only led to insignificant differences (up to 1%) in the resulting D_{rr}. This shows that this effect is small and easy to overlook. However, in a statistical sense, it has a significant impact as it eventually leads to margination. The main argument which shows that the platelet margination cannot be the sole result of diffusive flux is that the gradient of the diffusivity is positive from the centre of the channel towards the wall up until R = 0.7 [see, e.g., Fig. 9(b)]. The net flux contribution in the radial direction is proportional to $-\frac{\partial D_{rr}}{\partial r}$, which drives platelets inwards. Since the actual overall motion of the platelets points to the other direction, towards the wall, it must be governed by a stronger effect.

The shape of the platelet radial drift velocity (Fig. 10) shows resemblance to the hematocrit gradient, suggesting that the change in hematocrit levels has a larger influence on the platelet motion than the increase of shear rate. The magnitude of the drift increases slightly with the increase of average flow velocity; however, in agreement with previous experimental findings using tracer particles,[33] it increases more substantially with the increase of hematocrit. This further indicates the important role of the hematocrit profile in relation to platelet margination.

This study relies on several major assumptions. The results are devised using straight vessel sections, and therefore, the extended diffusive flux model is expected to require additional terms in bifurcations and in highly curved sections. For the shear rate and hematocrit, the typical physiologic range of small vessels was investigated. A different transport behaviour is expected[13,73] in the case of high hematocrit (>50%) or shear rate (>4000 s^{-1}). Furthermore, we employed a cytoplasmic viscosity ratio of $\Lambda = 1$. de Haan *et al.*[11] showed that this results in less than 5% difference in the displacement during cell collisions for shear rates <4000 s^{-1}; hence, this effect is neglected. Finally, the plasma is modelled as a Newtonian fluid. Recent studies[64,77] demonstrated that plasma can display strain hardening due to the contained protein chains. While this effect requires further investigation, de Haan *et al.*[11] also demonstrated that the local elongation rate stays below the strain hardening threshold for cell collisions in shear rate below 1000 s^{-1}.

With the advance of high-performance cellular modelling tools, such as HemoCell, large-scale investigations of cellular flow systems containing gradients are becoming available. Based on the evaluation of simulated cell trajectories, we proposed an extension to the diffusive flux model. It incorporates a more accurate approximation of the cell collision frequency and displacement, by allowing the collision cross section of the cells to change as a function of the local shear rate. According to our findings, this extension is important when describing cellular flows above the shear rate of 100 s^{-1}. Therefore, it allows for a better description of particle transport processes under the flow conditions appearing in real blood vessels. Furthermore, the results suggest that in vascular blood flows the radial migration of cells towards the wall is primarily dependent on the local hematocrit gradient. This is an important pointer in the development of the platelet margination theory.

ACKNOWLEDGMENTS

This work was supported by the European Union Horizon 2020 research and innovation programme under Grant Agreement No. 675451 (CompBioMed project) and Grant Agreement No. 777072 (Insist project). This work was sponsored by NWO Exacte Wetenschappen (Physical Sciences) for the use of supercomputer facilities, with financial support from the Nederlandse Organisatie voor Wetenschappelijk Onderzoek (Netherlands Organization for Science Research, NWO).

REFERENCES

[1] B. Davies and T. Morris, "Physiological parameters in laboratory animals and humans," Pharm. Res. **10**(7), 1093–1095 (1993).
[2] D. Boal and D. H. Boal, *Mechanics of the Cell* (Cambridge University Press, 2012).
[3] P. C.-H. Chan and L. G. Leal, "The motion of a deformable drop in a second-order fluid," J. Fluid Mech. **92**(1), 131–170 (1979).
[4] M. Loewenberg and E. J. Hinch, "Collision of two deformable drops in shear flow," J. Fluid Mech. **338**, 299–315 (1997).
[5] J. P. Mills, L. Qie, M. Dao, C. T. Lim, and S. Suresh, "Nonlinear elastic and viscoelastic deformation of the human red blood cell with optical tweezers," Mol. Cell. Biomech. **1**(3), 169–180 (2004).
[6] H. Zhao, A. P. Spann, and E. S. G. Shaqfeh, "The dynamics of a vesicle in a wall-bound shear flow," Phys. Fluids **23**(12), 121901 (2011).
[7] K. Klapcsik and F. Hegedűs, "The effect of high viscosity on the evolution of the bifurcation set of a periodically excited gas bubble," Chaos, Solitons Fractals **104**, 198–208 (2017).
[8] R. Toy, E. Hayden, C. Shoup, H. Baskaran, and E. Karathanasis, "The effects of particle size, density and shape on margination of nanoparticles in microcirculation," Nanotechnology **22**(11), 115101 (2011).
[9] A. Kumar and M. D. Graham, "Segregation by membrane rigidity in flowing binary suspensions of elastic capsules," Phys. Rev. E **84**(6), 066316 (2011).
[10] A. Kumar, R. G. Henríquez Rivera, and M. D. Graham, "Flow-induced segregation in confined multicomponent suspensions: Effects of particle size and rigidity," J. Fluid Mech. **738**, 423–462 (2014).
[11] M. de Haan, G. Zavodszky, V. Azizi, and A. Hoekstra, "Numerical investigation of the effects of red blood cell cytoplasmic viscosity contrasts on single cell and bulk transport behaviour," Appl. Sci. **8**(9), 1616 (2018).
[12] M. Abkarian and A. Viallat, "Vesicles and red blood cells in shear flow," Soft Matter **4**(4), 653–657 (2008).
[13] X. Grandchamp, G. Coupier, A. Srivastav, C. Minetti, and T. Podgorski, "Lift and down-gradient shear-induced diffusion in red blood cell suspensions," Phys. Rev. Lett. **110**, 108101 (2013).
[14] R. Fahraeus and T. Lindqvist, "The viscosity of the blood in narrow capillary tubes," Am. J. Physiol.-Legacy Content **96**(3), 562–568 (1931).
[15] R. P. Axel, D. Neuhaus, and P. Gaehtgens, "Blood viscosity in tube flow: Dependence on diameter and hematocrit," Am. J. Physiol. **263**(6), H1770–H1778 (1992).
[16] T. W. Secomb, "Blood flow in the microcirculation," Annu. Rev. Fluid Mech. **49**, 443–461 (2017).
[17] E. C. Eckstein, D. G. Bailey, and A. H. Shapiro, "Self-diffusion of particles in shear flow of a suspension," J. Fluid Mech. **79**(1), 191–208 (1977).
[18] P. Olla, "The lift on a tank-treading ellipsoidal cell in a shear flow," J. Phys. II **7**(10), 1533–1540 (1997).
[19] P. AMM Aarts, S. A. T. van den Broek, G. W. Prins, G. D. C. Kuiken, J. J. Sixma, and R. M. Heethaar, "Blood platelets are concentrated near the wall and red blood cells, in the center in flowing blood," Arteriosclerosis: Off. J. Am. Heart Assoc., Inc. **8**(6), 819–824 (1988).
[20] H. L. Goldsmith, G. R. Cokelet, and P. Gaehtgens, "Robin fahraeus: Evolution of his concepts in cardiovascular physiology," Am. J. Physiol. Heart Circ. Physiol. **257**(3), H1005–H1015 (1989).
[21] P. Pranay, R. G. Henríquez-Rivera, and M. D. Graham, "Depletion layer formation in suspensions of elastic capsules in Newtonian and viscoelastic fluids," Phys. Fluids **24**(6), 061902 (2012).
[22] P. Balogh and P. Bagchi, "Analysis of red blood cell partitioning at bifurcations in simulated microvascular networks," Phys. Fluids **30**(5), 051902 (2018).
[23] E. Kaliviotis, J. M. Sherwood, and S. Balabani, "Local viscosity distribution in bifurcating microfluidic blood flows," Phys. Fluids **30**(3), 030706 (2018).
[24] K. Müller, D. A. Fedosov, and G. Gompper, "Margination of micro-and nano-particles in blood flow and its effect on drug delivery," Sci. Rep. **4**, 4871 (2014).
[25] T. Krüger, "Effect of tube diameter and capillary number on platelet margination and near-wall dynamics," Rheol. Acta **55**(6), 511–526 (2016).
[26] J. Tan, T. R. Sinno, and S. L. Diamond, "A parallel fluid–solid coupling model using lammps and palabos based on the immersed boundary method," J. Comput. Sci. **25**, 89–100 (2018).
[27] D. Leighton and A. Acrivos, "The shear-induced migration of particles in concentrated suspensions," J. Fluid Mech. **181**, 415–439 (1987).

[28]H. C. Berg, *Random Walks in Biology* (Princeton University Press, 1993).
[29]J. M. Higgins, D. T. Eddington, S. N. Bhatia, and L. Mahadevan, "Statistical dynamics of flowing red blood cells by morphological image processing," PLoS Comput. Biol. **5**(2), e1000288 (2009).
[30]F. R. Da Cunha and E. J. Hinch, "Shear-induced dispersion in a dilute suspension of rough spheres," J. Fluid Mech. **309**, 211–223 (1996).
[31]S. D. Hudson, "Wall migration and shear-induced diffusion of fluid droplets in emulsions," Phys. Fluids **15**(5), 1106–1113 (2003).
[32]H. L. Goldsmith and S. Spain, "Margination of leukocytes in blood flow through small tubes," Microvasc. Res. **27**(2), 204–222 (1984).
[33]S. Fitzgibbon, A. P. Spann, Q. M. Qi, and E. S. G. Shaqfeh, "*In vitro* measurement of particle margination in the microchannel flow: Effect of varying hematocrit," Biophys. J. **108**(10), 2601–2608 (2015).
[34]M. E. Fay, D. R. Myers, A. Kumar, C. T. Turbyfield, R. Byler, K. Crawford, R. G. Mannino, A. Laohapant, E. A. Tyburski, Y. Sakurai *et al.*, "Cellular softening mediates leukocyte demargination and trafficking, thereby increasing clinical blood counts," Proc. Natl. Acad. Sci. U. S. A. **113**(8), 1987–1992 (2016).
[35]A. L. Zydney and C. K. Colton, "Augmented solute transport in the shear flow of a concentrated suspension," PhysicoChem. Hydrodyn. **10**(1), 77–96 (1988).
[36]E. C. Eckstein and F. Belgacem, "Model of platelet transport in flowing blood with drift and diffusion terms," Biophys. J. **60**(1), 53 (1991).
[37]L. Crowl and A. L. Fogelson, "Analysis of mechanisms for platelet near-wall excess under arterial blood flow conditions," J. Fluid Mech. **676**, 348–375 (2011).
[38]T. Krüger, F. Varnik, and D. Raabe, "Efficient and accurate simulations of deformable particles immersed in a fluid using a combined immersed boundary lattice Boltzmann finite element method," Comput. Math. Appl. **61**(12), 3485–3505 (2011).
[39]K. Vahidkhah and P. Bagchi, "Microparticle shape effects on margination, near-wall dynamics and adhesion in a three-dimensional simulation of red blood cell suspension," Soft Matter **11**(11), 2097–2109 (2015).
[40]G. Závodszky, B. van Rooij, V. Azizi, and A. G. Hoekstra, "Cellular level *in-silico* modeling of blood rheology with an improved material model for red blood cells," Front. Physiol. **8**, 1–14 (2017).
[41]H. Zhao, E. S. G. Shaqfeh, and V. Narsimhan, "Shear-induced particle migration and margination in a cellular suspension," Phys. Fluids **24**(1), 011902 (2012).
[42]A. Kumar and M. D. Graham, "Margination and segregation in confined flows of blood and other multicomponent suspensions," Soft Matter **8**(41), 10536–10548 (2012).
[43]I. V. Pivkin and G. E. Karniadakis, "A new method to impose no-slip boundary conditions in dissipative particle dynamics," J. Comput. Phys. **207**(1), 114–128 (2005).
[44]D. A. Fedosov, B. Caswell, and G. E. Karniadakis, "Systematic coarse-graining of spectrin-level red blood cell models," Comput. Methods Appl. Mech. Eng. **199**(29-32), 1937–1948 (2010).
[45]R. J. Phillips, R. C. Armstrong, R. A. Brown, A. L. Graham, and J. R. Abbott, "A constitutive equation for concentrated suspensions that accounts for shear-induced particle migration," Phys. Fluids A **4**(1), 30–40 (1992).
[46]P. Kanehl and H. Stark, "Hydrodynamic segregation in a bidisperse colloidal suspension in microchannel flow: A theoretical study," J. Chem. Phys. **142**(21), 214901 (2015).
[47]P. R. Nott and J. F. Brady, "Pressure-driven flow of suspensions: Simulation and theory," J. Fluid Mech. **275**, 157–199 (1994).
[48]R. M. Miller and J. F. Morris, "Normal stress-driven migration and axial development in pressure-driven flow of concentrated suspensions," J. Non-Newtonian Fluid Mech. **135**(2-3), 149–165 (2006).
[49]See https://www.hemocell.eu for Hemocell–A high-performance framework for dense cellular suspension flows; accessed 10 January 2018.
[50]G. Závodszky and G. Paál, "Validation of a lattice Boltzmann method implementation for a 3D transient fluid flow in an intracranial aneurysm geometry," Int. J. Heat Fluid Flow **44**, 276–283 (2013).
[51]V. W. A. Tarksalooyeh, G. Závodszky, B. J. M. van Rooij, and A. G. Hoekstra, "Inflow and outflow boundary conditions for 2D suspension simulations with the immersed boundary lattice Boltzmann method," Comput. Fluids **172**, 312–317 (2018).
[52]G. Závodszky, G. Károlyi, and G. Paál, "Emerging fractal patterns in a real 3D cerebral aneurysm," J. Theor. Biol. **368**, 95–101 (2015).
[53]B. Czaja, G. Závodszky, V. A. Tarksalooyeh, and A. G. Hoekstra, "Cell-resolved blood flow simulations of saccular aneurysms: Effects of pulsatility and aspect ratio," J. R. Soc., Interface **15**(146), 20180485 (2018).
[54]L. Mountrakis, E. Lorenz, O. Malaspinas, S. Alowayyed, B. Chopard, and A. G. Hoekstra, "Parallel performance of an IB-LBM suspension simulation framework," J. Comput. Sci. **9**, 45–50 (2015).
[55]S. Alowayyed, G. Závodszky, V. Azizi, and A. G. Hoekstra, "Load balancing of parallel cell-based blood flow simulations," J. Comput. Sci. **24**, 1–7 (2018).
[56]R. Skalak, A. Tozeren, R. P. Zarda, and S. Chien, "Strain energy function of red blood cell membranes," Biophys. J. **13**(3), 245–264 (1973).
[57]M. Dao, J. Li, and S. Suresh, "Molecularly based analysis of deformation of spectrin network and human erythrocyte," Mater. Sci. Eng.: C **26**(8), 1232–1244 (2006).
[58]E. J. Carboni, B. H. Bognet, G. M. Bouchillon, A. L. Kadilak, L. M. Shor, M. D. Ward, and A. W. K. Ma, "Direct tracking of particles and quantification of margination in blood flow," Biophys. J. **111**(7), 1487–1495 (2016).
[59]V. Breedveld, D. Van Den Ende, M. Bosscher, R. J. J. Jongschaap, and J. Mellema, "Measurement of the full shear-induced self-diffusion tensor of noncolloidal suspensions," J. Chem. Phys. **116**(23), 10529–10535 (2002).
[60]H. L. Goldsmith, J. Marlow, and F. C. MacIntosh, "Flow behaviour of erythrocytes-i. Rotation and deformation in dilute suspensions," Proc. R. Soc. London, Ser. B **182**(1068), 351–384 (1972).
[61]M. E. Rosti, L. Brandt, and D. Mitra, "Rheology of suspensions of viscoelastic spheres: Deformability as an effective volume fraction," Phys. Rev. Fluids **3**(1), 012301 (2018).
[62]W. Yao, Z. Wen, Z. Yan, D. Sun, K. Weibo, L. Xie, and S. Chien, "Low viscosity Ektacytometry and its validation tested by flow chamber," J. Biomech. **34**(11), 1501–1509 (2001).
[63]R. M. MacMECCAN, J. R. Clausen, G. P. Neitzel, and C. K. Aidun, "Simulating deformable particle suspensions using a coupled lattice-Boltzmann and finite-element method," J. Fluid Mech. **618**, 13–39 (2009).
[64]M. Brust, C. Schaefer, R. Doerr, L. Pan, M. Garcia, P. E. Arratia, and C. Wagner, "Rheology of human blood plasma: Viscoelastic versus Newtonian behavior," Phys. Rev. Lett. **110**(7), 078305 (2013).
[65]N. O. Jaensson, M. A. Hulsen, and P. D. Anderson, "Direct numerical simulation of particle alignment in viscoelastic fluids," J. Non-Newtonian Fluid Mech. **235**, 125–142 (2016).
[66]H. L. Goldsmith and J. C. Marlow, "Flow behavior of erythrocytes. II. particle motions in concentrated suspensions of ghost cells," J. Colloid Interface Sci. **71**(2), 383–407 (1979).
[67]H. L. Goldsmith and V. T. Turitto, "Rheological aspects of thrombosis and haemostasis: Basic principles and applications. Icth-report–subcommittee on rheology of the international committee on thrombosis and haemostasis," Thromb. Haemostasis **55**(3), 415 (1986).
[68]M. Mehrabadi, D. N. Ku, and C. K. Aidun, "A continuum model for platelet transport in flowing blood based on direct numerical simulations of cellular blood flow," Ann. Biomed. Eng. **43**(6), 1410–1421 (2015).
[69]I. E. Zarraga and D. T. Leighton, Jr., "Normal stress and diffusion in a dilute suspension of hard spheres undergoing simple shear," Phys. Fluids **13**(3), 565–577 (2001).
[70]G. Drazer, J. Koplik, B. Khusid, and A. Acrivos, "Deterministic and stochastic behaviour of non-Brownian spheres in sheared suspensions," J. Fluid Mech. **460**, 307–335 (2002).
[71]R. Rusconi and H. A. Stone, "Shear-induced diffusion of platelike particles in microchannels," Phys. Rev. Lett. **101**(25), 254502 (2008).
[72]M. Saadatmand, T. Ishikawa, N. Matsuki, M. J. Abdekhodaie, Y. Imai, H. Ueno, and T. Yamaguchi, "Fluid particle diffusion through high-hematocrit blood flow within a capillary tube," J. Biomech. **44**(1), 170–175 (2011).
[73]L. Mountrakis, E. Lorenz, and A. G. Hoekstra, "Scaling of shear-induced diffusion and clustering in a blood-like suspension," Europhys. Lett. **114**(1), 14002 (2016).

[74]Q. M. Qi and E. S. G. Shaqfeh, "Theory to predict particle migration and margination in the pressure-driven channel flow of blood," Phys. Rev. Fluids **2**(9), 093102 (2017).
[75]N. Tateishi, Y. Suzuki, M. Soutani, and N. Maeda, "Flow dynamics of erythrocytes in microvessels of isolated rabbit mesentery: Cell-free layer and flow resistance," J. Biomech. **27**(9), 1119–1125 (1994).
[76]K. Vahidkhah, S. L. Diamond, and P. Bagchi, "Platelet dynamics in three-dimensional simulation of whole blood," Biophys. J. **106**(11), 2529–2540 (2014).
[77]S. Varchanis, Y. Dimakopoulos, C. Wagner, and J. Tsamopoulos, "How viscoelastic is human blood plasma?," Soft Matter **14**(21), 4238–4251 (2018).